Mononuclear Low-Spin 3:1-Type Iron(II) Complexes of 4-Substituted 3,5-Di-(2-pyridyl)- and 3-Phenyl-5-(2-pyridyl)-4H-1,2,4-triazoles

Julia Klingele, Harald Scherer, Marco Klingele

Zeitschrift für Anorganische und Allgemeine Chemie

Mononuclear Low-Spin 3:1-Type Iron(II) Complexes of 4-Substituted 3,5-Di-(2-pyridyl)- and 3-Phenyl-5-(2-pyridyl)-4H-1,2,4-triazoles

Journal:	*Zeitschrift für Anorganische und Allgemeine Chemie*
Manuscript ID:	zaac.200900137.R2
Wiley - Manuscript type:	Article
Date Submitted by the Author:	26-Apr-2009
Complete List of Authors:	Klingele, Julia; Albert-Ludwigs-Universität Freiburg, Institut für Anorganische und Analytische Chemie Scherer, Harald; Albert-Ludwigs-Universität Freiburg, Institut für Anorganische und Analytische Chemie Klingele, Marco; Albert-Ludwigs-Universität Freiburg, Institut für Anorganische und Analytische Chemie
Keywords:	Iron, 1,2,4-Triazoles, N ligands, X-Ray diffraction, NMR spectroscopy

Mononuclear Low-Spin 3:1-Type Iron(II) Complexes of 4-Substituted 3,5-Di-(2-pyridyl)- and 3-Phenyl-5-(2-pyridyl)-4*H*-1,2,4-triazoles

Julia Klingele*[a], Harald Scherer[a] and Marco H. Klingele[a]

* Dr. Julia Klingele

Email: julia.klingele@ac.uni-freiburg.de

[a] Institut für Anorganische und Analytische Chemie

Albert-Ludwigs-Universität Freiburg

Albertstr. 21

D-79104 Freiburg (Germany)

Fax: +49-(0)761-203-6001

Abstract: Two series of mononuclear 3:1-type iron(II) complexes have been obtained by the reaction of $Fe(ClO_4)_2 \cdot 6H_2O$ with nine previously reported 1,2,4-triazole-based ligands. The first series, $[Fe^{II}\mathbf{L}^{S}_3](ClO_4)_2 \cdot n H_2O$, is based on symmetrical 4-substituted 3,5-di-(2-pyridyl)-4*H*-1,2,4-triazoles where $\mathbf{L}^{S}$ = **medpt** [4-methyl-3,5-di-(2-pyridyl)-4*H*-1,2,4-triazole], **ibdpt** [4-isobutyl-3,5-di-(2-pyridyl)-4*H*-1,2,4-triazole], **pmdpt** [4-(4-methylphenyl)-3,5-di-(2-pyridyl)-4*H*-1,2,4-triazole], **pydpt** [3,5-di-(2-pyridyl)-4-(4-pyridyl)-4*H*-1,2,4-triazole] and **pldpt** [3,5-di-(2-pyridyl)-4-(1*H*-pyrrol-1-yl)-4*H*-1,2,4-triazole] whereas the complexes of the second series, $[Fe^{II}\mathbf{L}^{U}_3](ClO_4)_2 \cdot n H_2O$, incorporate unsymmetrical 4-substituted 3-phenyl-5-(2-pyridyl)-4*H*-1,2,4-triazoles with $\mathbf{L}^{U}$ = **meppt** [4-methyl-5-phenyl-3-(2-pyridyl)-4*H*-1,2,4-triazole], **ibppt** [4-isobutyl-3-phenyl-5-(2-pyridyl)-4*H*-1,2,4-triazole], **pmppt** [4-(4-methylphenyl)-3-phenyl-5-(2-pyridyl)-4*H*-1,2,4-triazole] and **pyppt** [3-phenyl-5-(2-pyridyl)-4-(4-pyridyl)-4*H*-1,2,4-triazole]. The complexes have been investigated by ^{1}H NMR spectroscopy and found to be in the low-spin state at room temperature. Single crystal X-ray diffraction studies of the complexes $[Fe^{II}(\mathbf{pmdpt})_3](ClO_4)_2 \cdot MeCN \cdot 0.5H_2O$ (**I**), $[Fe^{II}(\mathbf{ibdpt})_3](ClO_4)_2 \cdot 2H_2O$ (**II**) and $[Fe^{II}(\mathbf{ibppt})_3](BF_4)_2 \cdot 1.34MeOH \cdot 0.16H_2O$ (**III**) have revealed meridional arrangements of the ligands and distorted octahedral FeN_6 coordination environments about the respective low-spin iron(II) centres.

Keywords: Iron; 1,2,4-Triazoles; N ligands; X-Ray diffraction; NMR spectroscopy

Introduction

The occurrence of spin crossover (SCO) between a high-spin (HS) and a low-spin (LS) state in octahedral complexes of $3d^4$–$3d^7$ first row transition metal ions is a very attractive phenomenon, and a variety of applications, especially in the field of information technology, can be envisaged for such compounds [1–4]. Owing to this fact the SCO phenomenon [5, 6] has been intensively studied over the last few decades with research in this field focussing on iron(II) complexes [7–15]. As a result, a great variety of iron(II) SCO compounds [16–23] are now known, and, in fact, a "rule of thumb" has evolved over time for the selection of ligands suitable to form SCO complexes with iron(II) salts. Thus, N-heterocyclic donor ligands giving rise to a distorted octahedral coordination environment are particularly favourable [20, 24].

Among others, ligands based on the 1,2,4-triazole core have been found to form SCO compounds with iron(II) salts quite frequently [25–28]. In this context, iron(II) complexes of the neutral, potentially bis-bidentate ligand 4-amino-3,5-di-(2-pyridyl)-4*H*-1,2,4-triazole (**adpt**) have been studied extensively over the years [29–43]. In addition, reports of iron(II) complexes incorporating the closely related 4-(3-methylphenyl)-3,5-di-(2-pyridyl)-4*H*-1,2,4-triazole (**mmdpt**) [44], 4-(4-methylphenyl)-3,5-di-(2-pyridyl)-4*H*-1,2,4-triazole (**pmdpt**) [44] and 3,5-di-(2-pyridyl)-4-(1*H*-pyrrol-1-yl)-4*H*-1,2,4-triazole (**pldpt**) [42], i.e. derivatives of **adpt** formally derived by variation of the substituent on N^4 (Figure 1), have also appeared in the literature. However, all structurally characterised iron(II) complexes of these ligands reported to date are of the mononuclear *trans*-$[Fe^{II}\mathbf{L}_2Y_2]^{0/2+}$ [30, 32, 34, 35, 39, 41–44], mononuclear *cis*-$[Fe^{II}\mathbf{L}_2Y_2]$ [44] or dinuclear $[Fe^{II}_2\mathbf{L}_2Y_4]^{0/4+}$ type [42] and exhibit FeN_4Y_2 coordination environments, where Y denotes additional unidentate co-ligands, e.g. pseudo-halides, halides or solvent molecules. Complexes of the cationic mononuclear $[Fe^{II}\mathbf{L}_3]^{2+}$ type displaying FeN_6 coordination environments should be accessible by employing a 3:1 ligand-to-metal stoichiometry. In these complexes one of the two coordination pockets of each ligand remains uncoordinated. Although such complexes have been mentioned briefly in literature [23, 42], to the best of our knowledge no structural or analytical data for complexes of this type have been published so far.

((Insert Figure 1 here))

The symmetrical 4-substituted 3,5-di-(2-pyridyl)-4*H*-1,2,4-triazoles **medpt** [4-methyl-3,5-di-(2-pyridyl)-4*H*-1,2,4-triazole], **ibdpt** [4-isobutyl-3,5-di-(2-pyridyl)-4*H*-1,2,4-triazole] and **pydpt** [3,5-di-(2-pyridyl)-4-(4-pyridyl)-4*H*-1,2,4-triazole] as well as the connatural unsymmetrical ligands

meppt [4-methyl-5-phenyl-3-(2-pyridyl)-4*H*-1,2,4-triazole], **ibppt** [4-isobutyl-3-phenyl-5-(2-pyridyl)-4*H*-1,2,4-triazole], **pmppt** [4-(4-methylphenyl)-3-phenyl-5-(2-pyridyl)-4*H*-1,2,4-triazole] and **pyppt** [3-phenyl-5-(2-pyridyl)-4-(4-pyridyl)-4*H*-1,2,4-triazole], in which one of the two lateral 2-pyridyl substituents has been replaced by a phenyl group, were first described in 2004 [45] (Figure 1). Of these compounds only **pyppt** [46] and **ibdpt** [47, 48] have been used for the preparation of complexes. In this paper we report the synthesis and ^{1}H NMR spectroscopic study of the 3:1-type complexes $[Fe^{II}\mathbf{L}^{S}_3](ClO_4)_2{\cdot}nH_2O$, based on symmetrical 4-substituted 3,5-di-(2-pyridyl)-4*H*-1,2,4-triazoles, with $\mathbf{L}^{S}$ = **medpt**, **ibdpt**, **pmdpt**, **pydpt** and **pldpt** and of the corresponding 3:1-type complexes $[Fe^{II}\mathbf{L}^{U}_3](ClO_4)_2{\cdot}nH_2O$, derived from unsymmetrical 4-substituted 3-phenyl-5-(2-pyridyl)-4*H*-1,2,4-triazoles, where $\mathbf{L}^{U}$ = **meppt**, **ibppt**, **pmppt** and **pyppt**. In addition, we present the structural characterisation by X-ray diffraction of the first examples of such 3:1-type complexes, namely $[Fe^{II}(\mathbf{pmdpt})_3](ClO_4)_2{\cdot}MeCN{\cdot}0.5H_2O$ (**I**), $[Fe^{II}(\mathbf{ibdpt})_3](ClO_4)_2{\cdot}2H_2O$ (**II**) and $[Fe^{II}(\mathbf{ibppt})_3](BF_4)_2{\cdot}1.34MeOH{\cdot}0.16H_2O$ (**III**), the latter being the first structurally characterised complex of a 4-alkyl-3-phenyl-5-(2-pyridyl)-4*H*-1,2,4-triazole.

Results and Discussion

Synthesis of the Complexes

The complexes $[Fe^{II}\mathbf{L}^{S}_3](ClO_4)_2{\cdot}nH_2O$ and $[Fe^{II}\mathbf{L}^{U}_3](ClO_4)_2{\cdot}nH_2O$ were prepared in MeOH solution employing a ligand-to-metal molar ratio of 3:1. All reactions were performed in air at room temperature. Thus, addition of a solution of $Fe(ClO_4)_2{\cdot}6H_2O$ to a solution of the appropriate ligand $\mathbf{L}^{S}$ or $\mathbf{L}^{U}$ resulted in the formation of red precipitates either immediately upon addition or after a few hours of stirring. The products were identified by elemental analysis as the desired 3:1-type complexes, showing a varying degree of hydration, the compositions being $[Fe^{II}(\mathbf{medpt})_3](ClO_4)_2{\cdot}4H_2O$, $[Fe^{II}(\mathbf{ibdpt})_3](ClO_4)_2{\cdot}H_2O$, $[Fe^{II}(\mathbf{pmdpt})_3](ClO_4)_2{\cdot}4H_2O$, $[Fe^{II}(\mathbf{pydpt})_3](ClO_4)_2{\cdot}2H_2O$, $[Fe^{II}(\mathbf{pldpt})_3](ClO_4)_2{\cdot}H_2O$, $[Fe^{II}(\mathbf{meppt})_3](ClO_4)_2{\cdot}2H_2O$, $[Fe^{II}(\mathbf{ibppt})_3](ClO_4)_2{\cdot}H_2O$, $[Fe^{II}(\mathbf{pmppt})_3](ClO_4)_2{\cdot}4H_2O$ and $[Fe^{II}(\mathbf{pyppt})_3](ClO_4)_2{\cdot}4H_2O$, respectively (Scheme 1). All complexes proved to be air stable once formed and, except for $[Fe^{II}(\mathbf{pyppt})_3](ClO_4)_2{\cdot}4H_2O$, could be recrystallised from EtOH/MeOH to obtain pure microcrystalline materials in ca. 40–65 % yield. The attempted recrystallisation of the latter compound from EtOH/MeOH resulted in the formation of a yet unidentified yellow solid. An analytically pure sample of $[Fe^{II}(\mathbf{pyppt})_3](ClO_4)_2{\cdot}4H_2O$ was obtained straight from the reaction mixture instead.

((Insert Scheme 1 here))

^{1}H NMR spectroscopic studies

The complexes $[Fe^{II}\mathbf{L}^{S}_3](ClO_4)_2{\cdot}nH_2O$ and $[Fe^{II}\mathbf{L}^{U}_3](ClO_4)_2{\cdot}nH_2O$ as well as the corresponding free ligands were studied by ^{1}H NMR spectroscopy in CD_3CN solution. All complexes were revealed to be diamagnetic, i.e. in the LS state at or slightly above room temperature. Dissociation of the complexes was found to be reasonably low under these conditions, although line broadening was observed. Unequivocal assignments of the signals were obtained by a combination of one- and two-dimensional NMR experiments. ^{1}H NMR chemical shifts of the complexes and the corresponding free ligands are listed in Table 1, the numbering scheme employed for signal assignment is given in Figure 2.

((Insert Table 1 here))

The ^{1}H NMR chemical shifts of the 2-pyridyl substituents of the free ligands are almost identical (±0.05 ppm) for each pair of compounds bearing the same substituent on N^4, i.e. replacement of one of the two 2-pyridyl groups by a phenyl group does not affect the chemical shifts of the remaining pyridine ring. Instead, the chemical shifts of the signals observed for the lateral 2-pyridyl group(s) correlate strongly with the nature of the substituent on N^4 of the triazole core. Hence, in the spectra of the 4-alkyl-substituted ligands **medpt**, **ibdpt**, **meppt** and **ibppt** the signals of the 2-pyridyl groups are shifted downfield compared to the corresponding signals of the 4-(hetero)aryl-substituted ligands **pmdpt**, **pydpt**, **pmppt** and **pyppt**. The greatest effect is observed for H^1 adjacent to the pyridine nitrogen atom. In the spectra of **medpt**, **ibdpt**, **meppt** and **ibppt** it appears at $\delta \approx 8.70$ ppm while it is observed at $\delta \approx 8.30$ ppm for **pmdpt**, **pydpt**, **pmppt** and **pyppt**. This downfield shift is also observed for H^2 ($\delta \approx 7.45$ ppm vs. 7.30 ppm) and H^3 ($\delta \approx 7.90$ ppm vs. 7.85 ppm), albeit here it is far less pronounced. The signal for H^1 ($\delta = 8.46$ ppm) of the 4-(1*H*-pyrrol-1-yl)-substituted ligand **pldpt** appears at an intermediate chemical shift compared to the 4-alkyl- and 4-(hetero)aryl-substituted derivatives. This is also the case for H^2 ($\delta = 7.40$ ppm) while the chemical shift of H^3 ($\delta = 7.85$ ppm) is in good agreement with the values observed for the 4-(hetero)aryl-substituted ligands. For the 4-alkyl-substituted ligands **medpt**, **ibdpt**, **meppt** and **ibppt** the signal for H^4 is observed at $\delta \approx 8.20$ ppm, for **pmdpt** and **pmppt** at $\delta \approx 7.95$ ppm and for **pydpt** and **pyppt** at $\delta \approx 8.15$ ppm. With a chemical shift of $\delta = 7.83$ ppm for **pldpt**, the H^4 signal appears at even

higher field than for the 4-(hetero)aryl-substituted ligands. Within the group of the unsymmetrical ligands **meppt**, **ibppt**, **pmppt** and **pyppt** the same trend of a general downfield shift of the ^{1}H resonances in the spectra of the 4-alkyl-substituted ligands compared to those of the 4-(hetero)aryl-substituted congeners can also be observed looking at the signals of the lateral 2-phenyl group.

((Insert Figure 2 here))

In the complexes of the unsymmetrical ligands $\mathbf{L^U}$ = **meppt**, **ibppt**, **pmppt** and **pyppt** the nitrogen donor of the sole lateral 2-pyridyl group is inevitably coordinated to the iron(II) centre, which results in significant changes of the ^{1}H chemical shifts of the pyridine ring. Again, 4-alkyl- and 4-(hetero)aryl-substituted ligands have to be distinguished. In the complexes of the 4-alkyl-substituted ligands **meppt** and **ibppt** the most pronounced effect is observed for H^1, which is shifted upfield by 0.84 and 0.81 ppm, respectively, compared to the free ligands. The resonances for H^2 remain almost unchanged upon complexation, whereas the signals for H^3 and H^4 are observed with a slight downfield shift. A totally different pattern is observed for complexes of the 4-(hetero)aryl-substituted ligands **pmppt** and **pyppt**. Here, the H^1 signals are affected only slightly by complexation, the signals for H^2 are observed with a moderate downfield shift and the H^3 resonances remain practically unchanged upon complexation. The H^4 signals display the greatest effect with upfield shifts of 0.80 and 0.90 ppm for **pmppt** and **pyppt**, respectively. For the unsymmetrical ligands **meppt**, **ibppt**, **pmppt** and **pyppt** there is basically no effect of complexation observable in the chemical shifts of H^{10} and H^{11} of the phenyl group. However, the signal for H^9, closest to the triazole core, is shifted upfield upon coordination by 0.14 and 0.17 ppm for **meppt** and **ibppt**, respectively, while it remains virtually unchanged for **pmppt** and **pyppt**.

The symmetrical ligands $\mathbf{L^S}$ = **medpt**, **ibdpt**, **pmdpt**, **pydpt** and **pldpt** offer two identical bidentate binding sites. In the 3:1-type complexes of these ligands only one of these binding sites is actually coordinated to the iron(II) centre whereas the other one remains unoccupied. However, the coordination-induced shift behaviour of the coordinating 2-pyridyl groups is the same for both the unsymmetrical and the symmetrical ligands. Thus, the coordinating 2-pyridyl groups can be easily identified by comparison with the characteristic shifts observed for the $\mathbf{L^U}$ ligand series (Table 1).

Once again the changes in chemical shifts upon complexation of the 4-(1*H*-pyrrol-1-yl)-substituted ligand **pldpt** differ from both the behaviour of the 4-alkyl- and the 4-(hetero)aryl-substituted ligands. Thus, contrary to the other ligands, the H^1 signal appears with a considerable downfield shift of 0.63 ppm. As with the 4-(hetero)aryl-substituted ligands **pmdpt**, **pmppt**, **pydpt** and **pyppt**,

the largest shift is observed for the H^4 signal with an upfield shift of 0.80 ppm. Similarly, the H^2 signal is shifted downfield by 0.53 ppm. On the other hand, the behaviour of the H^3 signal resembles that of the 4-alkyl-substituted ligands **medpt**, **meppt**, **ibdpt** and **ibppt** in that it is shifted downfield by 0.15 ppm. In the complexes of the symmetrical ligands **medpt**, **ibdpt**, **pmdpt**, **pydpt** and **pldpt** the chemical shifts observed for H^{10}, H^{11} and H^{12} of the uncoordinated 2-pyridyl group remain virtually unchanged while the signal for H^9, closest to the triazole core, experiences an upfield shift of 0.32, 0.39, 0.11, 0.19 and 0.08 ppm, respectively, compared to the free ligand.

The observed differences in ^{1}H chemical shifts and their different variation upon coordination between the 4-alkyl- and 4-(hetero)aryl-substituted ligands indicate that the respective electronic systems are different in the free ligands and, in addition, are modified differently by complexation. This effect is, not surprisingly, most pronounced for the coordinated 2-pyridyl group.

Figure 3 depicts the ^{1}H NMR spectra of the free ligand **medpt** (top) as well as of the complexes $[Fe^{II}(\mathbf{medpt})_3](ClO_4)_2{\cdot}4H_2O$ (middle) and $[Fe^{II}(\mathbf{meppt})_3](ClO_4)_2{\cdot}2H_2O$ (bottom). As can be seen nicely here, the spectrum of the **medpt** complex (middle) is composed of two sets of signals, i.e. the signals of both the uncoordinated (top) and the coordinated (bottom) 2-pyridyl groups. The strong upfield shift of H^1 as well as the moderate downfield shifts of H^3 and H^4 of the coordinated 2-pyridyl group are clearly visible while at the same time the H^2 signal does not shift. Similarly, it can be seen that for the uncoordinated 2-pyridyl group the signals for $H^1 \rightarrow H^{12}$, $H^2 \rightarrow H^{11}$ and $H^3 \rightarrow H^{10}$ experience practically no shift whereas the signal for $H^4 \rightarrow H^9$ is shifted upfield. Figure 4 gives an analogous representation for **pydpt** (top), $[Fe^{II}(\mathbf{pydpt})_3](ClO_4)_2{\cdot}2H_2O$ (middle) and $[Fe^{II}(\mathbf{pyppt})_3](ClO_4)_2{\cdot}4H_2O$ (bottom).

((Insert Figure 3 here))

((Insert Figure 4 here))

Single crystal X-ray diffraction studies

Although crystalline bulk material could be obtained for all ClO_4^- complexes, except for $[Fe^{II}(\mathbf{pyppt})_3](ClO_4)_2{\cdot}4H_2O$, by recrystallisation from EtOH/MeOH or other techniques, e.g. slow evaporation, solvent diffusion or vapour diffusion, it turned out to be surprisingly difficult to grow single crystals suitable for X-ray diffraction. Within the $[Fe^{II}\mathbf{L}^{S}_3](ClO_4)_2{\cdot}n H_2O$ series, only

$[Fe^{II}(\mathbf{pmdpt})_3](ClO_4)_2{\cdot}4H_2O$ and $[Fe^{II}(\mathbf{ibdpt})_3](ClO_4)_2{\cdot}H_2O$ afforded suitable material while no single crystals from other $[Fe^{II}\mathbf{L}^{S}_3](ClO_4)_2{\cdot}nH_2O$ complexes could be obtained. Thus, $[Fe^{II}(\mathbf{pmdpt})_3](ClO_4)_2{\cdot}MeCN{\cdot}0.5H_2O$ (**I**) and $[Fe^{II}(\mathbf{ibdpt})_3](ClO_4)_2{\cdot}2H_2O$ (**II**) were obtained by vapour diffusion of TBME into a MeCN solution and by slow evaporation of an EtOH solution of the complex, respectively. Given these difficulties with the ClO_4^- complexes, the corresponding BF_4^- compounds were prepared following the general procedure described in the Experimental Section using $Fe(BF_4)_2{\cdot}6H_2O$ instead of $Fe(ClO_4)_2{\cdot}6H_2O$. The BF_4^- complexes were not characterised but only used for crystallisation experiments. And indeed, vapour diffusion of TBME into the MeOH reaction mixture prepared from $Fe(BF_4)_2{\cdot}6H_2O$ and **ibppt** in a 1:3 molar ratio afforded single crystals of $[Fe^{II}(\mathbf{ibppt})_3](BF_4)_2{\cdot}1.34MeOH{\cdot}0.16H_2O$ (**III**).

((Insert Figure 5 here))

Single crystal X-ray diffraction ultimately confirmed the expected 3:1-type structures of the compounds. The **pmdpt** complex **I** and the **ibppt** complex **III** crystallise in the monoclinic space group *C*2/*c* while the **ibdpt** complex **II** crystallises in the monoclinic space group *P*2(1)/*c*. For all three complexes the coordination sphere about the respective iron(II) centre is best described as N_6 distorted octahedral. The coordinating bidentate binding pockets of the ligands in all three structures are arranged in such a way, that equivalent donor atoms of different ligands are located on opposite corners of the coordination octahedron as often as possible, i.e. twice [$N_{pyr}(201)\cdots N_{pyr}(301)$ and $N_{trz}(102)\cdots N_{trz}(202)$] instead of not at all. Thus, the *mer* conformation is adopted by all three complexes in the solid state (Figures 5–7).

((Insert Figure 6 here))

The average Fe–N distances and N–Fe–N angles of the three complexes compare well (Tables 2 and 3). The former are typical for LS iron(II) complexes displaying FeN_6 coordination [20, 28] but are slightly longer then the corresponding distances observed in the related 2:1-type SCO complexes $[Fe^{II}(\mathbf{adpt})_2(TCNQ)_2]$ (TCNQ = 7,7',8,8'-tetracyanoquinodimethane) [30] and $[Fe^{II}(\mathbf{adpt})_2\{N(CN)_2\}_2]$ [43] in their LS forms. The Fe–N_{pyr} distances [1.989(4)–1.992(4) (**I**), 1.976(4)–1.985(4) Å (**II**) and 1.984(3)–1.992(3) Å (**III**)] are longer than the Fe–N_{trz} distances [1.920(4)–1.936(4) Å (**I**), 1.918(3)–1.926(4) (**II**) and 1.920(3)–1.945(3) (**III**)]. The same trend has been observed in the related neutral 2:1-type complexes $[Fe^{II}(\mathbf{adpt})_2(NCS)_2]$ [32, 35], $[Fe^{II}(\mathbf{adpt})_2(NCSe)_2]$ [32, 35], $[Fe^{II}(\mathbf{adpt})_2\{N(CN)_2\}_2]$ [34, 39, 43], $[Fe^{II}(\mathbf{adpt})_2\{C(CN)_3\}_2]$ [41], $[Fe^{II}(\mathbf{adpt})_2(TCP\text{-}OMe)_2]$ (TCP-OMe = 1,1,3,3-tetracyano-2-methoxypropenide) [41],

$[Fe^{II}(\mathbf{adpt})_2(TCP\text{-}OEt)_2]$ (TCP-OEt = 1,1,3,3-tetracyano-2-ethoxypropenide) [41], $[Fe^{II}(\mathbf{pmdpt})_2(NCS)_2]$ [44] and $[Fe^{II}(\mathbf{mmdpt})_2(NCS)_2]$ [44] as well as in the cationic 2:1-type complex $[Fe^{II}(\mathbf{adpt})_2py_2]^{2+}$ [42]. In all three complexes the coordinated pyridine and the triazole rings are co-planar [0.8(2)–3.2(2)° (**I**), 4.0(3)–6.0(3)° (**II**) and 2.9(3)–5.3(2)° (**III**)]. Interestingly, in the **ibdpt** complex **II** the non-coordinating pyridine rings of the three ligands show only relatively small deviations from co-planarity to the adjacent triazole ring [1.5(3), 6.3(5) and 20.9(2)°] whereas in the other two complexes the non-coordinating pyridine and the phenyl ring, respectively, are tilted quite significantly against the central triazole ring [11.1(3), 42.9(2) and 87.3(3)° for the **pmdpt** complex **I**; 39.8(3), 46.9(2) and 49.2(2)° for the **ibppt** complex **III**]. In complexes **I** and **II** of the symmetrical ligands **pmdpt** and **ibdpt**, respectively, the nitrogen atoms of the non-coordinating pyridine rings are twisted away from the metal centre and point towards the complex's outer sphere. This is the same behaviour as usually observed in mononuclear complexes of 4-substituted 3,5-di-(2-pyridyl)-4*H*-1,2,4-triazoles [49]. Crystallographic data for complexes **I**–**III** are summarised in Table 4.

((Insert Figure 7 here))

((Insert Table 2 here))

((Insert Table 3 here))

((Insert Table 4 here))

Experimental Section

General remarks. $Fe(ClO_4)_2{\cdot}6H_2O$ and $Fe(BF_4)_2{\cdot}6H_2O$ were purchased from Aldrich and used as received. All solvents used were laboratory reagent grade. The ligands **pldpt** [50, 51] as well as **medpt**, **ibdpt**, **pmdpt**, **pydpt**, **meppt**, **ibppt**, **pmppt** and **pyppt** [45] were prepared as described in the literature. All manipulations were carried out in air. Melting points were determined using a Setaram DSC 131 evo differential scanning calorimeter. Elemental analyses were carried out with an Elementar Vario EL analyzer. IR spectra were recorded over the range 4000–400 cm^{-1} using a Nicolet Magna 760 FTIR spectrometer. NMR spectra were recorded on a Bruker AVANCE II 400 WB spectrometer with a 5 mm ATM BBFO probe head, the decoupler coil tuned to the frequency of ^1H (400.17 MHz, 12 μs 90° pulse) and the detector coil tuned to the frequency of ^{13}C (100.62

MHz, 10.2 µs 90° pulse). ^{1}H and ^{13}C chemical shifts are given relative to TMS using the residual solvent peak as the reference signal. Unless stated otherwise, all NMR measurements were carried out at 25°C. Two-dimensional ^{1}H,^{1}H COSY, ^{13}C,^{1}H HSQC and ^{13}C,^{1}H HMBC spectra were carried out in order to allow for unambiguous peak assignment. However, due to the short T_2 relaxation time of the majority of ^{1}H resonances, not all ^{13}C signals of quaternary carbon atoms, especially those belonging to the triazole core, could be detected by long-range correlations. UV/Vis spectra were recorded on a JASCO V-570 UV/Vis/NIR spectrophotometer over the range 200–870 nm using 0.1 and 0.01 mM MeCN solutions of the complexes.

General procedure. A solution of $Fe(ClO_4)_2{\cdot}6H_2O$ (36.3 mg, 0.10 mmol) in MeOH (5 ml) was added to a solution of the appropriate ligand (0.30 mmol) in MeOH (5 ml) at room temperature. The resulting complexes precipitated either immediately upon addition or after a few hours of stirring as red solids, which were filtered off, washed with MeOH (2 ml) and dried in vacuo. Pure materials were obtained straight from the reaction mixture or by recrystallisation from EtOH/MeOH.

Caution! While no problems were encountered in the course of this work, ClO_4^- salts are potentially explosive and should be handled with appropriate care.

$[Fe^{II}(medpt)_3](ClO_4)_2{\cdot}4H_2O$. Prepared from **medpt** (71.2 mg) in 52 % yield (71.3 mg). M.p. 227°C. Elemental analysis (%) found: C 45.33, H 3.91, N 20.16; calcd. for $C_{39}H_{41}N_{15}O_{12}Cl_2Fe$ (1038.60 g mol^{-1}): C 45.10, H 3.98, N 20.23. IR (diamond ATR): *mu* = 3396.0 (br), 3060.6 (br), 1614.3, 1587.4 (s), 1587.6, 1539.4, 1521.3, 1448.5 (vs), 1426.7 (s), 1373.3, 1287.6, 1251.8, 1152.6, 1081.0 (vs, br), 992.5, 797.4 (s), 786.4 (s), 745.7 (s), 730.4, 703.2 (s), 680.7, 622.3 (vs), 601.6, 524.6, 498.5, 469.8 (br), 418.9 cm^{-1}. ^{1}H NMR (400.13 MHz, CD_3CN): δ = 4.57 (br, 3 H, CH_3), 7.46 (br, 1 H, 5-Py$_{coord}H$), 7.49 (br, 1 H, 5-PyH), 7.87 (br, 1 H, 3-PyH), 7.88 (br, 1 H, 4-PyH), 7.93 (br, 1 H, 6-Py$_{coord}H$), 8.12 (br, 1 H, 4-Py$_{coord}H$), 8.40 (br, 1 H, 3-Py$_{coord}H$), 8.73 (br, 1 H, 6-PyH) ppm. ^{13}C NMR (100.62 MHz, CD_3CN): δ = 34.8 (CH_3), 123.0 (3-Py$_{coord}C$), 124.4 (3-PyC), 125.6 (5-PyC), 125.9 (5-Py$_{coord}C$), 137.6 (4-PyC), 138.3 (4-Py$_{coord}C$), 149.5 (6-PyC), 156.8 (6-Py$_{coord}C$) ppm. UV/Vis (MeCN): λ_{max} (ε) = 255 (31500), 292 (66100), 487 nm (9720 M^{-1} cm^{-1}).

$[Fe^{II}(ibdpt)_3](ClO_4)_2{\cdot}H_2O$. Prepared from **ibdpt** (83.8 mg) in 52 % yield (61.7 mg). M.p. 234°C. Elemental analysis (%) found: C 52.03, H 5.00, N 18.18; calcd. for $C_{48}H_{53}N_{15}O_9Cl_2Fe$ (1110.80 g mol^{-1}): C 51.90, H 4.81, N 18.91. IR (diamond ATR): *mu* = 2961.3 (br), 2931.9 (br), 2875.4 (br), 1608.9, 1586.5, 1572.5, 1521.1, 1508.0, 1486.5, 1465.9, 1446.6 (vs), 1424.2 (s), 1390.7, 1376.9, 1280.4, 1243.7, 1155.0, 1078.2 (vs, br), 994.9 (s), 946.8, 928.2, 886.9 (br), 793.2 (s), 781.3, 740.3

(s), 712.8 (s), 689.8, 620.7 (vs), 599.9, 515.3, 456.8, 430.1 cm^{-1}. ^{1}H NMR (400.13 MHz, CD_3CN): δ = 0.81 [br, 6 H, $CH_2CH(CH_3)_2$], 2.13 [br, 1 H, $CH_2CH(CH_3)_2$], 5.12 [br, 2 H, $CH_2CH(CH_3)_2$], 7.44 (br, 1 H, 5-$Py_{coord}H$), 7.49 (br, 1 H, 5-Py*H*), 7.81 (br, 1 H, 3-Py*H*), 7.86 (br, 1 H, 4-Py*H*), 7.88 (br, 1 H, 6-$Py_{coord}H$), 8.14 (br, 1 H, 4-$Py_{coord}H$), 8.32 (br, 1 H, 3-$Py_{coord}H$), 8.72 (br, 1 H, 6-Py*H*) ppm. ^{13}C NMR (100.62 MHz, CD_3CN): δ = 18.4 [$CH_2CH(CH_3)_2$], 29.5 ($CH_2CH(CH_3)_2$], 52.4 [$CH_2CH(CH_3)_2$], 123.1 (3-$Py_{coord}C$), 124.5 (3-Py*C*), 125.4 (5-Py*C*), 125.8 (5-$Py_{coord}C$), 137.7 (4-Py*C*), 138.3 (4-$Py_{coord}C$), 149.2 (6-Py*C*), 156.5 (6-$Py_{coord}C$) ppm. UV/Vis (MeCN): λ_{max} (ε) = 257 (29200), 292 (61800), 490 nm (9510 M^{-1} cm^{-1}).

$[Fe^{II}(pmdpt)_3](ClO_4)_2 \cdot 4H_2O$. Prepared from **pmdpt** (94.0 mg) in 51 % yield (64.2 mg). M.p. 236°C. Elemental analysis (%) found: C 53.91, H 4.11, N 16.39; calcd. for $C_{57}H_{53}N_{15}O_{12}Cl_2Fe$ (1266.89 g mol^{-1}): C 54.04, H 4.22, N 16.58. IR (diamond ATR): *mu* = 3567.0 (br), 3081.7 (br), 1610.9, 1512.3 (s), 1489.6, 1444.8 (vs), 1424.7 (s), 1362.5, 1291.2, 1254.7, 1182.5, 1151.5, 1075.7 (vs, br), 995.0, 832.7, 793.1 (s), 780.6 (s), 746.5 (s), 712.2 (s), 639.0, 619.0 (vs), 527.1, 497.7, 457.6 cm^{-1}. ^{1}H NMR (400.13 MHz, CD_3CN): δ = 2.50 (s, 3 H, CH_3), 7.00 (m, 1 H, 3-$Py_{coord}H$), 7.38 (m, 1 H, 5-Py*H*), 7.48 (br, 5 H, 2-$Ph_{Me}H$, 3-$Ph_{Me}H$, 5-$Ph_{Me}H$, 6-$Ph_{Me}H$ and 5-$Py_{coord}H$), 7.82 (br, 3 H, 3-Py*H*, 4-Py*H* and 4-$Py_{coord}H$), 8.15 (br, 1 H, 6-$Py_{coord}H$), 8.34 (m, 1 H, 6-Py*H*) ppm. ^{13}C NMR (100.62 MHz, CD_3CN): δ = 20.5 (CH_3), 122.4 (3-$Py_{coord}C$), 124.6 (3-Py*C*), 127.5 (2-$Ph_{Me}C$, 6-$Ph_{Me}C$), 125.3 (5-Py*C*), 126.0 (5-$Py_{coord}C$), 130.5 (3-$Ph_{Me}C$, 5-$Ph_{Me}C$), 137.6 (4-Py*C*), 137.6 (4-$Py_{coord}C$), 149.6 (6-Py*C*), 156.8 (6-$Py_{coord}C$) ppm. UV/Vis (MeCN): λ_{max} (ε) = 259 (34500), 290 (57700), 490 nm (10460 M^{-1} cm^{-1}).

$[Fe^{II}(pydpt)_3](ClO_4)_2 \cdot 2H_2O$. Prepared from **pydpt** (90.1 mg) in 57 % yield (67.8 mg). M.p. 223°C. Elemental analysis (%) found: C 51.76, H 3.17, N 21.29; calcd. for $C_{51}H_{40}N_{18}O_{10}Cl_2Fe$ (1191.75 g mol^{-1}): C 51.40, H 3.38, N 21.16. IR (diamond ATR): *mu* = 3072.8 (br), 1585.3 (s), 1516.9 (s), 1486.2, 1446.5 (vs), 1416.9 (s), 1361.5, 1289.2, 1253.5, 1217.8, 1154.7, 1080.4 (br, vs), 991.6 (s), 836.5, 793.1, 745.3, 725.8, 686.0, 641.4, 619.3 (s), 517.4 (br), 458.5 cm^{-1}. ^{1}H NMR (400.13 MHz, CD_3CN_3): δ = 7.13 (br, 1 H, 3-$Py_{coord}H$), 7.38 (br, 1 H, 5-Py*H*), 7.52 (br, 1 H, 5-$Py_{coord}H$), 7.65 (br, 2 H, 3'- and 5'-Py*H*), 7.85 (m, 2 H, 4-$Py_{coord}H$ and 4-Py*H*), 7.92 (br, 1 H, 3-Py*H*), 8.18 (br, 1 H, 6-$Py_{coord}H$), 8.27 (br, 1 H, 6-Py*H*), 8.93 (br, 2 H, 2'- and 6'-Py*H*) ppm. ^{13}C NMR (100.62 MHz, $CDCl_3$): δ = 122.5 (3'- and 5'-Py*C*), 123.0 (3-$Py_{coord}C$), 124.3 (3-Py*C*), 125.6 (5-Py*C*), 127.0 (5-$Py_{coord}C$), 137.5 (4-Py*C*), 138.6 (4-$Py_{coord}C$), 149.1 (6-Py*C*), 152.1 (2'- and 6'-Py*C*), 157.4 (6-$Py_{coord}C$) ppm. UV/Vis (MeCN): λ_{max} (ε) = 259 (36600), 291 (59400), 490 nm (10400 M^{-1} cm^{-1}).

[Fe^{II}(pldpt)$_3$](ClO$_4$)$_2$·H$_2$O. Prepared from **pldpt** (86.5 mg) in 65 % yield (73.8 mg). M.p. 222°C. Elemental analysis (%) found: C 50.52, H 3.34, N 22.75; calcd. for $C_{48}H_{38}N_{18}O_9Cl_2Fe$ (1137.70 g mol^{-1}): C 50.67, H 3.37, N 22.16. IR (diamond ATR): *mu* = 3079.6 (br), 1610.8, 1588.2, 1572.3, 1539.9, 1475.7, 1465.9, 1448.1 (s), 1431.9, 1334.8, 1285.8, 1252.4, 1083.3 (vs, br), 1069.7 (vs, br), 1004.6 (s), 991.4 (s), 911.4, 791.4, 781.2 (s), 727.0 (vs), 693.0, 651.2 (s), 619.2 (vs), 571.5, 521.0, 407.4 cm^{-1}. ^{1}H NMR (400.13 MHz, CD_3CN): δ = 6.52 (m, 2 H, 3-Pl*H* and 4-Pl*H*), 7.03 (br, 1 H, 3-Py$_{coord}$*H*), 7.23 (m, 2 H, 2-Pl*H* and 5-Pl*H*), 7.45 (br, 1 H, 5-Py*H*), 7.75 (br, 1 H, 3-Py*H*), 7.87 (br, 1 H, 4-Py*H*), 7.93 (br, 1 H, 5-Py$_{coord}$*H*), 8.00 (br, 1 H, 4-Py$_{coord}$*H*), 8.48 (br, 1 H, 6-Py*H*), 9.09 (br, 1 H, 6-Py$_{coord}$*H*) ppm. ^{13}C NMR (100.62 MHz, CD_3CN): δ = 110.3 (3-Pl*C* and 4-Pl*C*) 121.5 (2-Pl*C* and 5-Pl*C*), 124.0 (3-Py*C*), 124.9 (3-Py$_{coord}$*C*), 126.1 (5-Py*C*), 131.2 (5-Py$_{coord}$*C*),137.5 (4-Py*C*), 139.5 (4-Py$_{coord}$*C*), 150.3 (6-Py*C*) ppm, 157.3 (6-Py$_{coord}$*C*). UV/Vis (MeCN): λ_{max} (ε) = 250 (30500), 289 (58800), 487 nm (8850 M^{-1} cm^{-1}).

[Fe^{II}(meppt)$_3$](ClO$_4$)$_2$·2H$_2$O. Prepared from **meppt** (70.9 mg) in 40 % yield (39.7 mg). M.p. 206°C. Elemental analysis (%) found: C 50.53, H 3.79, N 16.68; calcd. for $C_{42}H_{40}N_{12}O_{10}Cl_2Fe$ (999.61 g mol^{-1}): C 50.47, H 4.03, N 16.81. IR (diamond ATR): *mu* = 3060.4 (br), 1611.0, 1533.1 (br), 1495.9, 1466.9 (s), 1443.4 (s), 1426.0, 1362.9, 1251.3, 1075.8 (vs, br), 1022.5, 988.8, 929.5, 885.8, 773.7 (s), 752.9 (s), 733.0, 697.1 (s), 666.5, 620.7 (vs), 607.0, 520.6, 492.9, 458.3, 406.1 cm^{-1}. ^{1}H NMR (400.13 MHz, CD_3CN): δ = 4.13 (s, 3 H, C*H*$_3$), 7.47 (m, 1 H, 5-Py*H*), 7.58 (m, 4 H, 2-, 3-, 5- and 6-Ph*H*), 7.59 (m, 1 H, 4-Ph*H*), 7.96 (m, 1 H, 6-Py*H*), 8.09 (m, 1 H, 4-Py*H*), 8.35 (m, 1 H, 3-Py*H*) ppm. ^{13}C NMR (100.62 MHz, CD_3CN): δ = 34.0 (*C*H$_3$), 122.7 (3-Py*C*), 126.1 (5-Py*C*), 129.2 (2-, 3-, 5- and 6-Ph*C*), 131.3 (4-Ph*C*), 138.0 (4-Py*C*), 156.9 (6-Py*C*) ppm. UV/Vis (MeCN): λ_{max} (ε) = 234 (31100), 256 (31700), 287 (50800), 487 nm (9820 M^{-1} cm^{-1}).

[Fe^{II}(ibppt)$_3$](ClO$_4$)$_2$·H$_2$O. Prepared from **ibppt** (83.5 mg) in 64 % yield (70.6 mg). M.p. 225°C. Elemental analysis (%) found: C 54.94, H 5.23, N 14.78; calcd. for $C_{51}H_{56}N_{12}O_9Cl_2Fe$ (1107.83 g mol^{-1}): C 55.29, H 5.10, N 15.17. IR (diamond ATR): *mu* = 2962.4 (br), 2933.7 (br), 2876.9 (br), 1608.7 (s), 1516.3 (s), 1487.4, 1466.8 (vs), 1444.5 (s), 1393.1, 1373.0, 1279.5, 1237.7, 1075.1 (vs, br), 991.9, 931.1, 881.4, 819.5, 779.2 (s), 749.4 (s), 728.8 (s), 699.9 (s), 676.1, 620.9 (vs), 520.4, 457.0, 432.1, 413.8 cm^{-1}. ^{1}H NMR (400.13 MHz, CD_3CN): δ = 0.66 [br, 6 H, $CH_2CH(CH_3)_2$], 2.01 [br, 1 H, $CH_2CH(CH_3)_2$], 4.42 [br, 2 H, $CH_2CH(CH_3)_2$], 7.45 (br, 1 H, 5-Py*H*), 7.50 (br, 2 H, 2- and 6-Ph*H*), 7.55 (m, 2 H, 3- and 5-Ph*H*), 7.60 (m, 1 H, 4-Ph*H*), 7.88 (br, 1 H, 6-Py*H*), 8.10 (br, 1 H, 4-Py*H*), 8.22 (br, 1 H, 3-Py*H*) ppm. ^{13}C NMR (100.62 MHz, CD_3CN): δ = 18.4 [$CH_2CH(CH_3)_2$], 29.0 [$CH_2CH(CH_3)_2$], 52.6 [$CH_2CH(CH_3)_2$], 122.8 (3-Py*C*), 125.9 (5-Py*C*), 129.1 (3- and 5-Ph*C*), 129.5

(2- and 6-Ph*C*), 131.1 (4-Ph*C*), 138.4 (4-Py*C*), 156.4 (6-Py*C*) ppm. UV/Vis (MeCN): λ_{max} (ε) = 231 (30500), 253 (29400), 286 (46900), 489 nm (10120 M^{-1} cm^{-1}).

$[Fe^{II}(pmppt)_3](ClO_4)_2 \cdot 4H_2O$. Prepared from **pmppt** (93.7 mg) in 58 % yield (73.2 mg). M.p. 222°C. Elemental analysis (%) found: C 57.01, H 4.26, N 13.17; calcd. for $C_{60}H_{56}N_{12}O_{12}Cl_2Fe$ (1263.93 g mol^{-1}): C 57.02, H 4.47, N 13.30. IR (diamond ATR): *mu* = 3063.1 (br), 1609.9, 1513.9 (s), 1488.4, 1465.4 (vs), 1441.1 (s), 1355.7, 1290.4, 1181.7, 1078.7 (vs, br), 1026.2, 989.8, 927.1, 833.7, 774.7 (s), 749.6, 711.9 (s), 696.5 (vs), 621.7 (vs), 528.8 (br), 458.5, 406.8 cm^{-1}. ^{1}H NMR (400.13 MHz, CD_3CN, 40°C): δ = 2.50 (s, 3 H, C*H*$_3$), 7.18 (br, 1 H, 3-Py*H*), 7.35 (m, 2 H, 3- and 5-Ph*H*), 7.41 (m, 2 H, 2- and 6-Ph*H*), 7.46 (m, 1 H, 4-Ph*H*), 7.49 (m, 2 H, 2- and 6-Ph$_{Me}$*H*), 7.52 (m, 2 H, 3- and 5-Ph$_{Me}$*H*), 7.58 (br, 1 H, 5-Py*H*), 7.83 (m, 1 H, 4-Py*H*), 8.38 (br, 1 H, 6-Py*H*) ppm. ^{13}C NMR (100.62 MHz, CD_3CN, 40°C): δ = 20.4 (*C*H$_3$), 123.0 (3-Py*C*), 125.3 (1-Ph*C*), 127.4 (2- and 6-Ph$_{Me}$*C*), 127.6 (5-Py*C*), 128.7 (3- and 5-Ph*C*), 128.8 (2- and 6-Ph*C*), 130.5 (1-Ph$_{Me}$*C*), 131.0 (4-Ph*C*), 131.4 (3- and 5-Ph$_{Me}$*C*), 138.1 (4-Py*C*), 142.6 (4-Ph$_{Me}$*C*), 147.4 (2-Py*C*), 156.8 (6-Py*C*), 161.5 (3-Tz*C*) ppm. UV/Vis (MeCN): λ_{max} (ε) = 289 (51200), 372 (3680), 491 nm (11020 M^{-1} cm^{-1}).

$[Fe^{II}(pyppt)_3](ClO_4)_2 \cdot 4H_2O$. Prepared from **pyppt** (89.8 mg) in 52 % yield (80.3 mg). M.p. 223°C. Elemental analysis (%) found: C 52.96, H 3.70, N 17.13; calcd. for $C_{54}H_{47}N_{15}O_{12}Cl_2Fe$ (1224.81 g mol^{-1}): C 52.95, H 3.87, N 17.15. IR (diamond ATR): *mu* = 3067.8 (br), 1610.3, 1582.1 (s), 1514.9, 1501.1, 1466.8 (s), 1440.8 (s), 1411.6 (s), 1352.0, 1092.6 (vs, br), 1075.4 (vs, br), 989.9, 927.5, 845.5, 773.4 (s), 750.3, 725.9, 711.2, 696.2 (vs), 674.4, 637.6 (s), 622.3 (vs), 517.8, 457.4, 403.2 cm^{-1}. ^{1}H NMR (400.13 MHz, CD_3CN_3): δ = 7.25 (m, 1 H, 3-Py*H*), 7.37–7.38 (m, 4 H, 2-, 3-, 5- and 6-Ph*H*), 7.48 (m, 1 H, 4-Ph*H*), 7.54 (m, 1 H, 5-Py*H*), 7.64 (br, 2 H, 3'- and 5'-Py*H*), 7.85 (m, 1 H, 4-Py*H*), 8.23 (br, 1 H, 6-Py*H*), 8.94 (m, 2 H, 2'- and 6'-Py*H*) ppm. ^{13}C NMR (100.62 MHz, $CDCl_3$): δ = 122.5 (3'- and 5'-Py*C*), 123.0 (3-Py*C*), 127.1 (5-Py*C*), 129.0 (2-, 3-, 5- and 6-Ph*C*), 131.3 (4-Ph*C*), 138.5 (4-Py*C*), 152.9 (2'- and 6'-Py*C*), 157.3 (6-Py*C*) ppm. UV/Vis (MeCN): λ_{max} (ε) = 287 (49100), 373 (3420), 491 nm (10000 M^{-1} cm^{-1}).

Crystal structure determinations. Single crystals of $[Fe^{II}(\mathbf{pmdpt})_3](ClO_4)_2 \cdot MeCN \cdot 0.5H_2O$ (**I**) were obtained by vapour diffusion of TBME into a MeCN solution of $[Fe^{II}(\mathbf{pmdpt})_3](ClO_4)_2 \cdot 4H_2O$ while crystals of $[Fe^{II}(\mathbf{ibdpt})_3](ClO_4)_2 \cdot 2H_2O$ (**II**) were grown by slow evaporation of an EtOH solution of $[Fe^{II}(\mathbf{ibdpt})_3](ClO_4)_2 \cdot H_2O$. Vapour diffusion of TBME into a MeOH reaction mixture prepared from $Fe(BF_4)_2 \cdot 6H_2O$ and **ibppt** in a 1:3 molar ratio as described above afforded single crystals of $[Fe^{II}(\mathbf{ibppt})_3](BF_4)_2 \cdot 1.34MeOH \cdot 0.16H_2O$ (**III**). Single crystal X-ray data were collected

using a Rigaku R-AXIS Spider IP area detector diffractometer using graphite-monochromated Mo-K_α radiation (λ = 0.71073 Å). The structures were solved by direct methods with SHELXS-97 [52] and refined against F^2 using all data by full-matrix least-squares techniques with SHELXL-97 [52]. All non-hydrogen atoms were refined anisotropically. All hydrogen atoms were placed in calculated positions using a riding model, except for those of water solvates, whose hydrogen atoms were located from the difference maps and refined with distance restraints. Disorder of the counter ions was modelled applying several geometrical constraints. CCDC-720147 (**I**), -720148 (**II**) and -720149 (**III**) contain the supplementary crystallographic data for this paper. These data can be obtained free of charge at www.ccdc.cam.ac.uk/data_request/cif or from the Cambridge Crystallographic Data Centre, 12 Union Road, Cambridge CB2 1EZ, UK.

Acknowledgements

Financial support to J.K. by the Schlieben-Lange Program (Ministry of Science, Research and the Arts Baden-Württemberg and European Social Fund) is gratefully acknowledged. J.K. thanks Prof. Dr. Ingo Krossing and Prof. Dr. Harald Hillebrecht for their generous and continuous support. Dr. Jens Geier is thanked for helpful advice on X-ray crystallography.

References

[1] J. Zarembowitch, O. Kahn, *New. J. Chem.* **1991**, *15*, 181–190.

[2] O. Kahn, J. Kröber, C. Jay, *Adv. Mater.* **1992**, *4*, 718–728.

[3] O. Kahn, C. J. Martinez, *Science* **1998**, *279*, 44–48.

[4] J.-F. Létard, P. Guionneau, L. Goux-Capes, *Top. Curr. Chem.* **2004**, *235*, 221–249.

[5] P. Gütlich, H. A. Goodwin, *Top. Curr. Chem.* **2004**, *233*, 1–47.

[6] J. A. Real, A. B. Gaspar, M. C. Muñoz, *Dalton Trans.* **2005**, 2062–2079.

[7] H. A. Goodwin, *Coord. Chem. Rev.* **1976**, *18*, 293–325.

[8] P. Gütlich, *Struct. Bonding* **1981**, *44*, 83–195.

[9] E. König, G. Ritter, S. K. Kulshreshtha, *Chem. Rev.* **1985**, *85*, 219–234.

[10] H. Toftlund, *Coord. Chem. Rev.* **1989**, *94*, 67–108.

[11] P. Gütlich, A. Hauser, *Coord. Chem. Rev.* **1990**, *97*, 1–22.

[12] A. Hauser, *Coord. Chem. Rev.* **1991**, *111*, 275–290.

[13] P. Gütlich, A. Hauser, H. Spiering, *Angew. Chem.* **1994**, *106*, 2109–2141; *Angew. Chem. Int. Ed. Engl.* **1994**, *33*, 2024–2054.

[14] P. Gütlich, Y. Garcia, H. A. Goodwin, *Chem. Soc. Rev.* **2000**, *29*, 419–427.

[15] S. V. Larionov, *Koord. Khim.* **2008**, *34*, 243–257; *Russ. J. Coord. Chem.* **2008**, *34*, 237–250.

[16] H. A. Goodwin, *Top. Curr. Chem.* **2004**, *233*, 59–90.

[17] P. J. van Koningsbruggen, *Top. Curr. Chem.* **2004**, *233*, 123–149.

[18] J. A. Real, A. B. Gaspar, M. C. Muñoz, P. Gütlich, V. Ksenofontov, H. Spiering, *Top. Curr. Chem.* **2004**, *233*, 167–193.

[19] Y. Garcia, V. Niel, M. C. Muñoz, J. A. Real, *Top. Curr. Chem.* **2004**, *233*, 229–257.

[20] P. Guionneau, M. Marchivie, G. Bravic, J.-F. Létard, D. Chasseau, *Top. Curr. Chem.* **2004**, *234*, 97–128.

[21] J. Kusz, P. Gütlich, H. Spiering, *Top. Curr. Chem.* **2004**, *234*, 129–153.

[22] M. A. Halcrow, *Polyhedron* **2007**, *26*, 3523–3576.

[23] K. S. Murray, *Eur. J. Inorg. Chem.* **2008**, 3101–3121.

[24] K. S. Murray, C. J. Kepert, *Top. Curr. Chem.* **2004**, *233*, 195–228.

[25] O. Kahn, E. Codjovi, *Philos. Trans. R. Soc. London Ser. A* **1996**, *354*, 359–379.

[26] J. G. Haasnoot in *Magnetism: A Supramolecular Function* (Ed.: O. Kahn), Kluwer, Dordrecht, **1996**, pp. 299–321.

[27] L. G. Lavrenova, S. V. Larionov, *Koord. Khim.* **1998**, *24*, 403–420; *Russ. J. Coord. Chem.* **1998**, *24*, 379–395.

[28] J. A. Kitchen, S. Brooker, *Coord. Chem. Rev.* **2008**, *252*, 2072–2092.

[29] J. P. Cornelissen, J. H. van Diemen, L. R. Groeneveld, J. G. Haasnoot, A. L. Spek, J. Reedijk, *Inorg. Chem.* **1992**, *31*, 198–202.

[30] P. J. Kunkeler, P. J. van Koningsbruggen, J. P. Cornelissen, A. N. van der Horst, A. M. van der Kraan, A. L. Spek, J. G. Haasnoot, J. Reedijk, *J. Am. Chem. Soc.* **1996**, *118*, 2190–2197.

[31] N. Moliner, M. C. Muñoz, P. J. van Koningsbruggen, J. A. Real, *Inorg. Chim. Acta* **1998**, *274*, 1–6.

[32] N. Moliner, M. C. Muñoz, S. Létard, J.-F. Létard, X. Solans, R. Burriel, M. Castro, O. Kahn, J. A. Real, *Inorg. Chim. Acta* **1999**, *291*, 279–288.

[33] J.-F. Létard, L. Capes, G. Chastanet, N. Moliner, S. Létard, J.-A. Real, O. Kahn, *Chem. Phys. Lett.* **1999**, *313*, 115–120.

[34] N. Moliner, A. B. Gaspar, M. C. Muñoz, V. Niel, J. Cano, J. A. Real, *Inorg. Chem.* **2001**, *40*, 3986–3991.

[35] A. B. Gaspar, M. C. Muñoz, N. Moliner, V. Ksenofontov, G. Levchenko, P. Gütlich, J. A. Real, *Monatsh. Chem.* **2003**, *134*, 285–294.

[36] M. Shakir, S. Parveen, N. Begum, Y. Azim, *Polyhedron* **2003**, *22*, 3181–3186.

[37] M. Shakir, S. Parveen, N. Begum, P. Chingsubam, *Transition Met. Chem.* **2004**, *29*, 196–199.

[38] P. Gütlich, A. B. Gaspar, V. Ksenofontov, Y. Garcia, *J. Phys. Condens. Matter* **2004**, *16*, S1087–S1108.

[39] S. Pillet, C. Lecomte, C. F. Sheu, Y. C. Lin, I. J. Hsu, Y. Wang, *J. Phys. Conf. Ser.* **2005**, *21*, 221–226.

[40] P. Gütlich, A. B. Gaspar, Y. Garcia, V. Ksenofontov, *C. R. Chimie* **2007**, *10*, 21–36.

[41] G. Dupouy, M. Marchivie, S. Triki, J. Sala-Pala, J.-Y. Salaün, C. J. Gómez-García, P. Guionneau, *Inorg. Chem.* **2008**, *47*, 8921–8931.

[42] J. A. Kitchen, A. Noble, C. D. Brandt, B. Moubaraki, K. S. Murray, S. Brooker, *Inorg. Chem.* **2008**, *47*, 9450–9458.

[43] C.-F. Sheu, S. Pillet, Y.-C. Lin, S.-M. Chen, I.-J. Hsu, C. Lecomte, Y. Wang, *Inorg. Chem.* **2008**, *47*, 10866–10874.

[44] D. Zhu, Y. Xu, Z. Yu, Z. Guo, H. Sang, T. Liu, X. You, *Chem. Mater.* **2002**, *14*, 838–843.

[45] M. H. Klingele, S. Brooker, *Eur. J. Org. Chem.* **2004**, 3422–3434.

[46] M. H. Klingele, S. Brooker, *Inorg. Chim. Acta* **2004**, *357*, 3413–3417.

[47] M. H. Klingele, P. D. W. Boyd, B. Moubaraki, K. S. Murray, S. Brooker, *Eur. J. Inorg. Chem.* **2005**, 910–918.

[48] M. H. Klingele, A. Noble, P. D. W. Boyd, S. Brooker, *Polyhedron* **2007**, *26*, 479–485.

[49] M. H. Klingele, S. Brooker, *Coord. Chem. Rev.* **2003**, *241*, 119–132.

[50] S. K. Mandal, H. J. Clase, J. N. Bridson, S. Ray, *Inorg. Chim. Acta* **1993**, *209*, 1–4.

[51] M. H. Klingele, P. D. W. Boyd, B. Moubaraki, K. S. Murray, S. Brooker, *Eur. J. Inorg. Chem.* **2006**, 573–589.

[52] G. M. Sheldrick, *Acta Crystallogr. Sect. A* **2008**, *64*, 112–122.

Captions

Figure 1. Structural drawings of the symmetrical ligands **adpt**, **pldpt**, **medpt**, **ibdpt**, **pydpt** and the unsymmetrical ligands **meppt**, **ibppt**, **pmppt** and **pyppt**.

Scheme 1. Preparation of the 3:1-type complexes $[Fe^{II}\mathbf{L}^{S}_{3}](ClO_4)_2{\cdot}nH_2O$ (X = N) and $[Fe^{II}\mathbf{L}^{U}_{3}](ClO_4)_2{\cdot}nH_2O$ (X = CH). The general formula depicts the *mer* conformation for these two series of complexes since this conformation is the one observed in the three structurally characterised examples reported herein.

Figure 2. Numbering scheme used in Table 1 for the assignment of ^{1}H NMR chemical shifts.

Figure 3. ^{1}H NMR spectra (CD_3CN, aromatic region) of **medpt** (top), $[Fe^{II}(\mathbf{medpt})_3](ClO_4)_2{\cdot}4H_2O$ (middle) and $[Fe^{II}(\mathbf{meppt})_3](ClO_4)_2{\cdot}2H_2O$ (bottom).

Figure 4. ^{1}H NMR spectra (CD_3CN, aromatic region) of **pydpt** (top), $[Fe^{II}(\mathbf{pydpt})_3](ClO_4)_2{\cdot}2H_2O$ (middle) and $[Fe^{II}(\mathbf{pyppt})_3](ClO_4)_2{\cdot}4H_2O$ (bottom).

Figure 5. View of the molecular structure of the cation of $[Fe^{II}(\mathbf{pmdpt})_3](ClO_4)_2{\cdot}MeCN{\cdot}0.5H_2O$ (**I**). Hydrogen atoms have been omitted for clarity.

Figure 6. View of the molecular structure of the cation of $[Fe^{II}(\mathbf{ibdpt})_3](ClO_4)_2{\cdot}2H_2O$ (**II**). Hydrogen atoms have been omitted for clarity.

Figure 7. View of the molecular structure of the cation of $[Fe^{II}(\mathbf{ibppt})_3](BF_4)_2{\cdot}1.34MeOH{\cdot}0.16H_2O$ (**III**). Hydrogen atoms have been omitted for clarity.

Tables

Table 1. Chemical shifts observed in the ^{1}H NMR spectra (CD_3CN) of the complexes $[Fe^{II}\mathbf{L}^{S}_3](ClO_4)_2{\cdot}nH_2O$ and $[Fe^{II}\mathbf{L}^{U}_3](ClO_4)_2{\cdot}nH_2O$ and of the corresponding free ligands.

Compound	H^1	H^2	H^3	H^4	H^9	H^{10}	H^{11}	H^{12}
medpt [a]	8.71	7.45	7.93	8.19	-/-	-/-	-/-	-/-
$[Fe^{II}(\mathbf{medpt})_3](ClO_4)_2{\cdot}4H_2O$	7.93	7.46	8.12	8.40	7.87	7.88	7.49	8.73
meppt [b]	8.70	7.43	7.92	8.22	7.72	7.56	7.56	-/-
$[Fe^{II}(\mathbf{meppt})_3](ClO_4)_2{\cdot}2H_2O$ [b]	7.96	7.47	8.09	8.35	7.58	7.58	7.59	-/-
ibdpt [a]	8.70	7.45	7.93	8.20	-/-	-/-	-/-	-/-
$[Fe^{II}(\mathbf{ibdpt})_3](ClO_4)_2{\cdot}H_2O$	7.88	7.44	8.14	8.32	7.81	7.86	7.49	8.72
ibppt [b]	8.69	7.44	7.92	8.22	7.67	7.56	7.56	-/-
$[Fe^{II}(\mathbf{ibppt})_3](ClO_4)_2{\cdot}H_2O$ [b]	7.88	7.45	8.10	8.22	7.50	7.55	7.60	-/-
pmdpt [a]	8.34	7.32	7.83	7.93	-/-	-/-	-/-	-/-
$[Fe^{II}(\mathbf{pmdpt})_3](ClO_4)_2{\cdot}4H_2O$	8.15	7.48	7.82	7.00	7.82	7.82	7.38	8.34
pmppt [b]	8.32	7.31	7.83	7.98	7.43	7.33	7.40	-/-
$[Fe^{II}(\mathbf{pmppt})_3](ClO_4)_2{\cdot}4H_2O$ [b]	8.38	7.58	7.83	7.18	7.41	7.35	7.46	-/-
pydpt [a]	8.26	7.33	7.88	8.11	-/-	-/-	-/-	-/-
$[Fe^{II}(\mathbf{pydpt})_3](ClO_4)_2{\cdot}2H_2O$	8.18	7.52	7.85	7.13	7.92	7.85	7.38	8.27
pyppt [b]	8.26	7.33	7.89	8.15	7.41	7.36	7.44	-/-
$[Fe^{II}(\mathbf{pyppt})_3](ClO_4)_2{\cdot}4H_2O$ [b]	8.23	7.54	7.85	7.25	7.37 / 7.38 [c]	7.37 / 7.38 [c]	7.48	-/-
pldpt [a]	8.46	7.40	7.85	7.83	-/-	-/-	-/-	-/-
$[Fe^{II}(\mathbf{pldpt})_3](ClO_4)2{\cdot}H_2O$	9.09	7.93	8.00	7.03	7.75	7.87	7.45	8.48

[a] H^1/H^{12}, H^2/H^{11}, H^3/H^{10} and H^4/H^9, respectively, are equivalent atoms and their chemical shifts are therefore identical.

[b] H^9/H^{13} and H^{10}/H^{12}, respectively, are equivalent atoms and their chemical shifts are therefore identical.

[c] The chemical shifts of H^9 and H^{10} are indistinguishable.

Table 2. Selected distances [Å] for $[Fe^{II}(\mathbf{pmdpt})_3](ClO_4)_2 \cdot MeCN \cdot 0.5H_2O$ (**I**), $[Fe^{II}(\mathbf{ibdpt})_3](ClO_4)_2 \cdot 2H_2O$ (**II**) and $[Fe^{II}(\mathbf{ibppt})_3](BF_4)_2 \cdot 1.34MeOH \cdot 0.16H_2O$ (**III**).

	I	II	III
Fe(1)–N(101)	1.989(4)	1.984(3)	1.988(3)
Fe(1)–N(102)	1.930(4)	1.926(4)	1.945(3)
Fe(1)–N(201)	1.992(4)	1.985(4)	1.992(3)
Fe(1)–N(202)	1.936(4)	1.919(4)	1.929(3)
Fe(1)–N(301)	1.991(4)	1.976(4)	1.984(3)
Fe(1)–N(302)	1.920(4)	1.918(3)	1.920(3)

Table 3. Selected angles [°] for $[Fe^{II}(\mathbf{pmdpt})_3](ClO_4)_2 \cdot MeCN \cdot 0.5H_2O$ (**I**), $[Fe^{II}(\mathbf{ibdpt})_3](ClO_4)_2 \cdot 2H_2O$ (**II**) and $[Fe^{II}(\mathbf{ibppt})_3](BF_4)_2 \cdot 1.34MeOH \cdot 0.16H_2O$ (**III**).

	I	II	III
N(101)–Fe(1)–N(102)	80.2(2)	80.2(1)	79.7(1)
N(101)–Fe(1)–N(201)	94.5(2)	92.6(1)	97.2(1)
N(101)–Fe(1)–N(202)	95.0(2)	96.0(1)	95.2(1)
N(101)–Fe(1)–N(301)	96.1(2)	97.7(1)	97.3(1)
N(101)–Fe(1)–N(302)	172.1(2)	175.7(2)	176.3(1)
N(102)–Fe(1)–N(201)	95.6(2)	97.7(2)	97.2(1)
N(102)–Fe(1)–N(202)	173.5(2)	175.4(2)	174.1(1)
N(102)–Fe(1)–N(301)	95.5(2)	90.5(2)	90.3(1)
N(102)–Fe(1)–N(302)	93.1(2)	96.1(2)	97.5(1)
N(201)–Fe(1)–N(202)	80.3(2)	79.8(2)	80.0(1)
N(201)–Fe(1)–N(301)	165.8(2)	167.8(1)	169.2(1)
N(201)–Fe(1)–N(302)	90.2(2)	90.2(1)	91.1(1)
N(202)–Fe(1)–N(301)	89.3(2)	92.6(2)	93.1(1)
N(202)–Fe(1)–N(302)	92.0(2)	87.8(2)	87.8(1)
N(301)–Fe(1)–N(302)	80.4(2)	79.9(1)	80.3(1)

Table 4. Crystallographic data for $[Fe^{II}(\mathbf{pmdpt})_3](ClO_4)_2 \cdot MeCN \cdot 0.5H_2O$ (**I**), $[Fe^{II}(\mathbf{ibdpt})_3](ClO_4)_2 \cdot 2H_2O$ (**II**) and $[Fe^{II}(\mathbf{ibppt})_3](BF_4)_2 \cdot 1.34MeOH \cdot 0.16H_2O$ (**III**).

	I	**II**	**III**
Empirical formula	$C_{59}H_{49}Cl_2FeN_{16}O_{8.5}$	$C_{48}H_{55}Cl_2FeN_{15}O_{10}$	$C_{52.34}H_{59.67}B_2F_8FeN_{12}O_{1.5}$
Formula weight [g mol^{-1}]	1244.89	1128.82	1110.31
Crystal system	monoclinic	monoclinic	monoclinic
Space group	*C*2/*c*	*P*2(1)/*c*	*P*2(1)/*c*
a [Å]	21.214(4)	17.378(3)	17.626(4)
b [Å]	20.901(4)	15.436(3)	15.616(3)
c [Å]	26.424(5)	20.963(4)	20.980(4)
α [°]	90	90	90
β [°]	95.93(3)	105.21(3)	102.50(3)
γ [°]	90	90	90
V [Å^3]	11654(4)	5426(2)	5638(2)
Z	8	4	4
$\rho_{calcd.}$ [g cm^{-3}]	1.419	1.382	1.308
μ [mm^{-1}]	0.422	0.446	0.343
Temperature [K]	100(2)	173(2)	150(2)
F(000)	5144	2352	2311
Crystal colour and shape	red plate	red plate	red plate
Crystal size [mm^3]	0.22 × 0.13 × 0.04	0.51 × 0.25 × 0.05	0.25 × 0.15 × 0.07
$\Theta_{min.}$ / $\Theta_{max.}$ [°]	3.03 / 26.37	3.02 / 24.71	3.04 / 27.48
h	–26 → 26	–20 → 20	–22 → 22
k	–26 → 26	–18 → 18	–19 → 20
l	–33 → 32	–24 → 24	–27 → 27
Reflections collected	74988	27621	100799
Independent reflections	11902 [R_{int} = 0.1672]	8695 [R_{int} = 0.0531]	12892 [R_{int}= 0.0649]
Completeness to $\Theta_{max.}$ [%]	99.8	94.0	99.8
Data / restraints / parameters	11902 / 66 / 922	8695 / 21 / 680	12892 / 79 / 731
GOOF	1.023	1.047	1.085
*R*1 / *wR*2 [$I > 2\sigma(I)$]	0.0795 / 0.1662	0.0640 / 0.1628	0.0845 / 0.2459
*R*1 / *wR*2 (all data)	0.1683 / 0.2032	0.0959 / 0.1898	0.1145 / 0.2762
Max. peak / hole [e Å^{-3}]	0.610 / –0.411	1.267 / –0.586	1.079 / –0.850

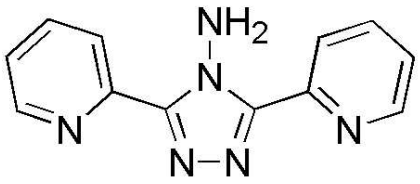

adpt

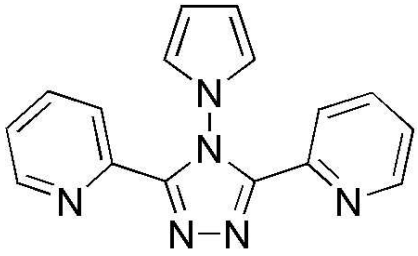

pldpt

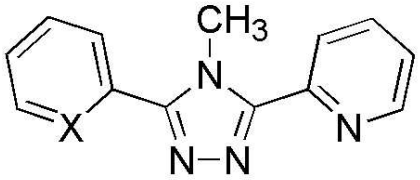

X = N:**medpt**
X = CH: **meppt**

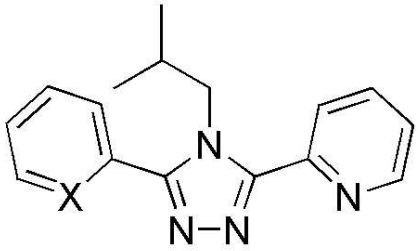

X = N: **ibdpt**
X = CH: **ibppt**

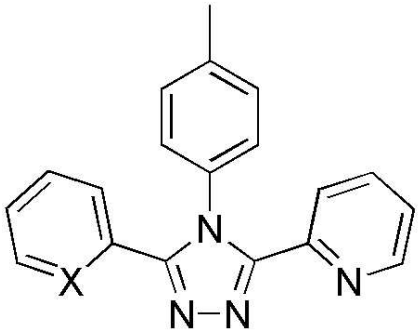

X = N: **pmdpt**
X = CH: **pmppt**

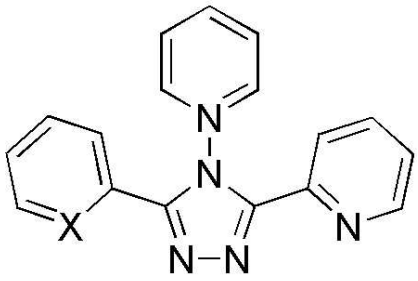

X = N: **pydpt**
X = CH: **pyppt**

84x109mm (300 x 300 DPI)

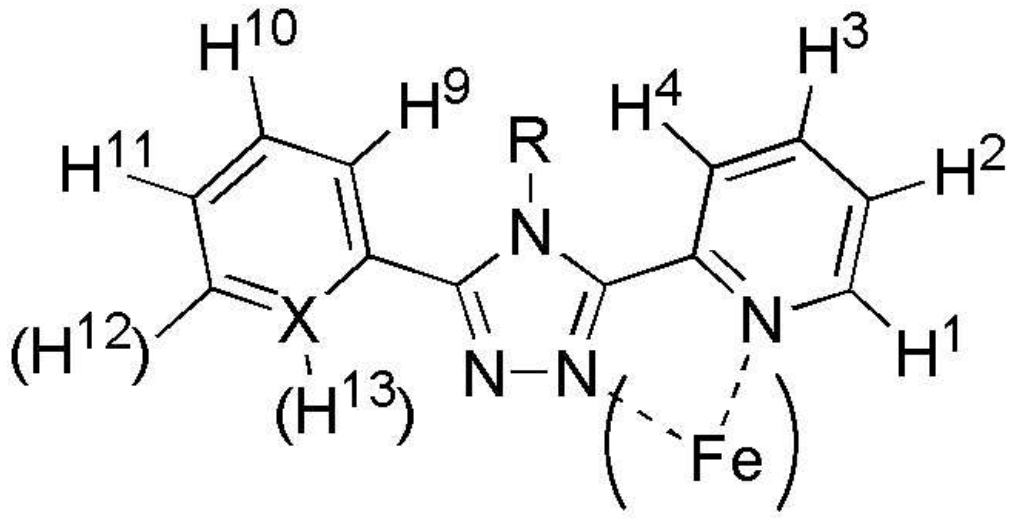

55x28mm (300 x 300 DPI)

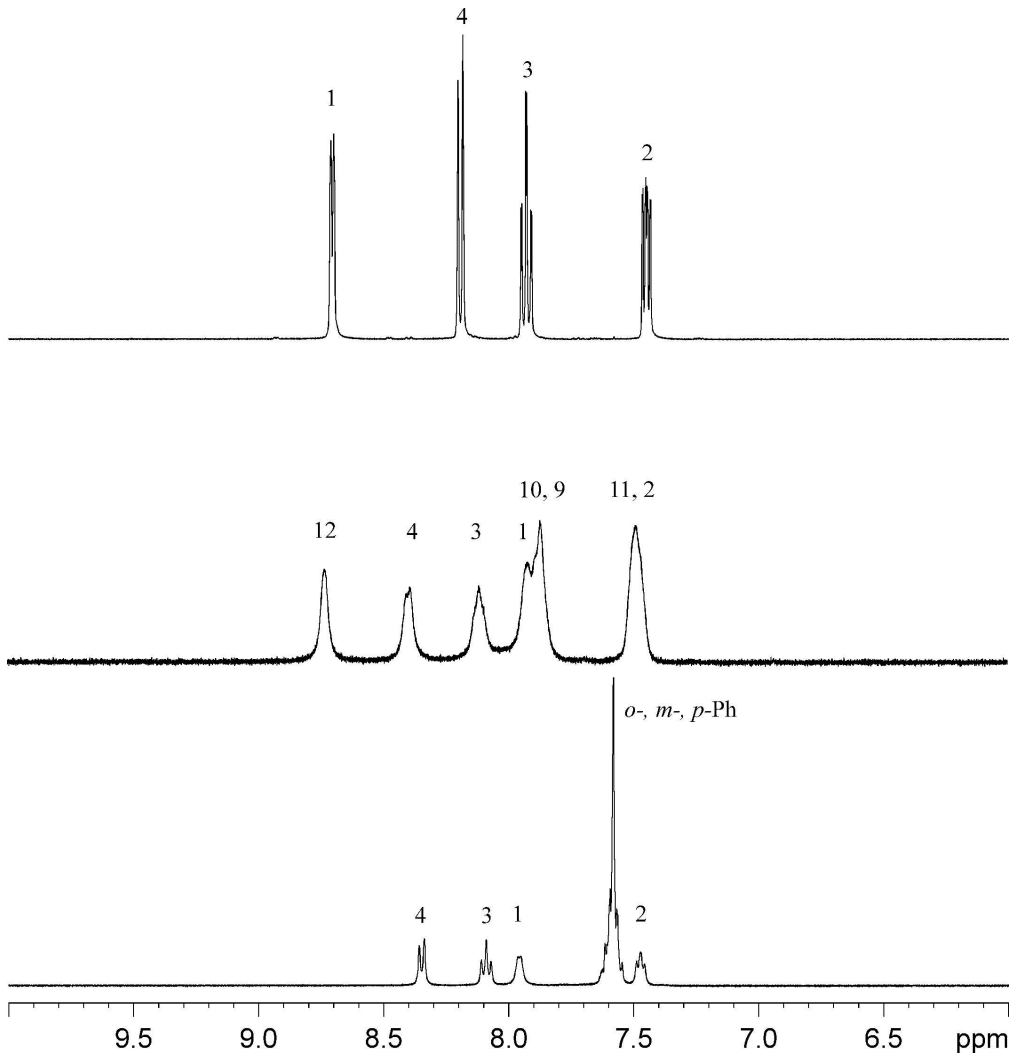
4
3
1
2
10, 9
11, 2
12
4
3
1
o-, m-, p-Ph
4
3
1
2
9.5
9.0
8.5
8.0
7.5
7.0
6.5
ppm

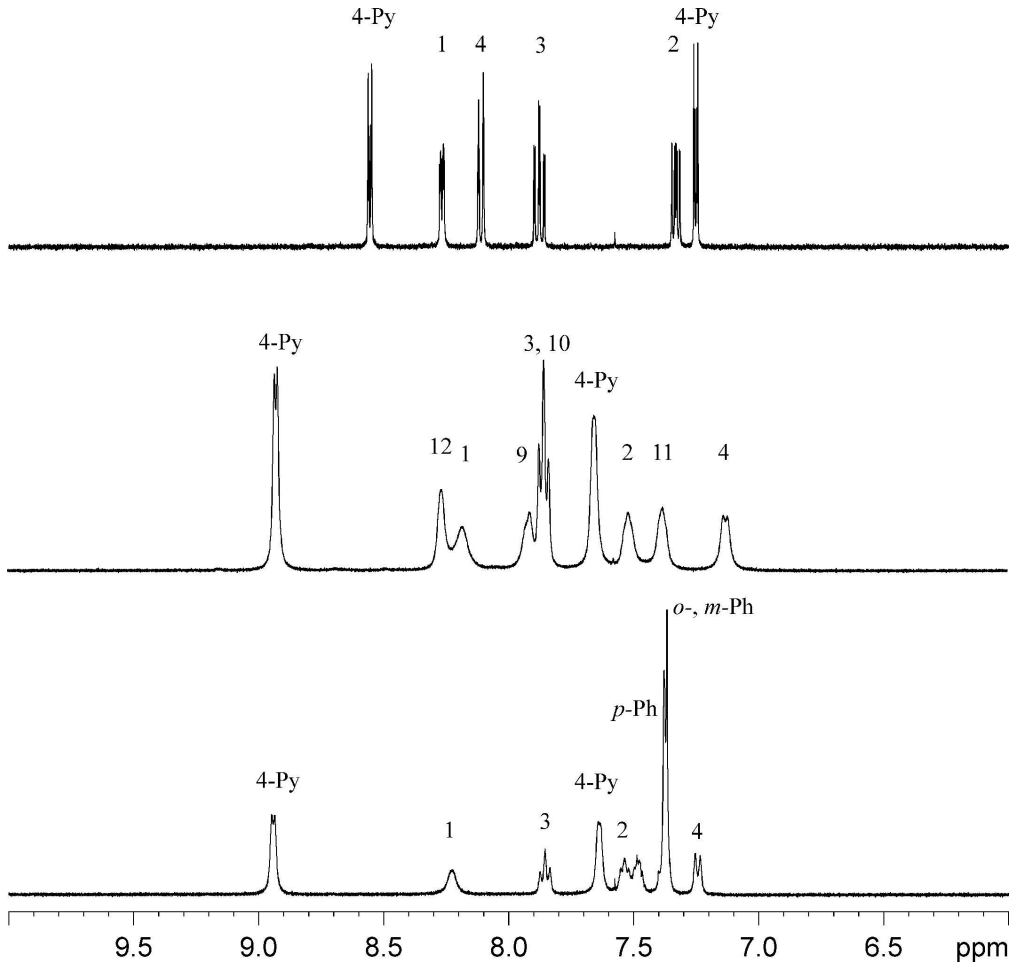
4-Py
1
4
3
4-Py
2
4-Py
3, 10
4-Py
12
1
9
2
11
4
o-, m-Ph
p-Ph
4-Py
4-Py
1
3
2
4
9.5
9.0
8.5
8.0
7.5
7.0
6.5
ppm

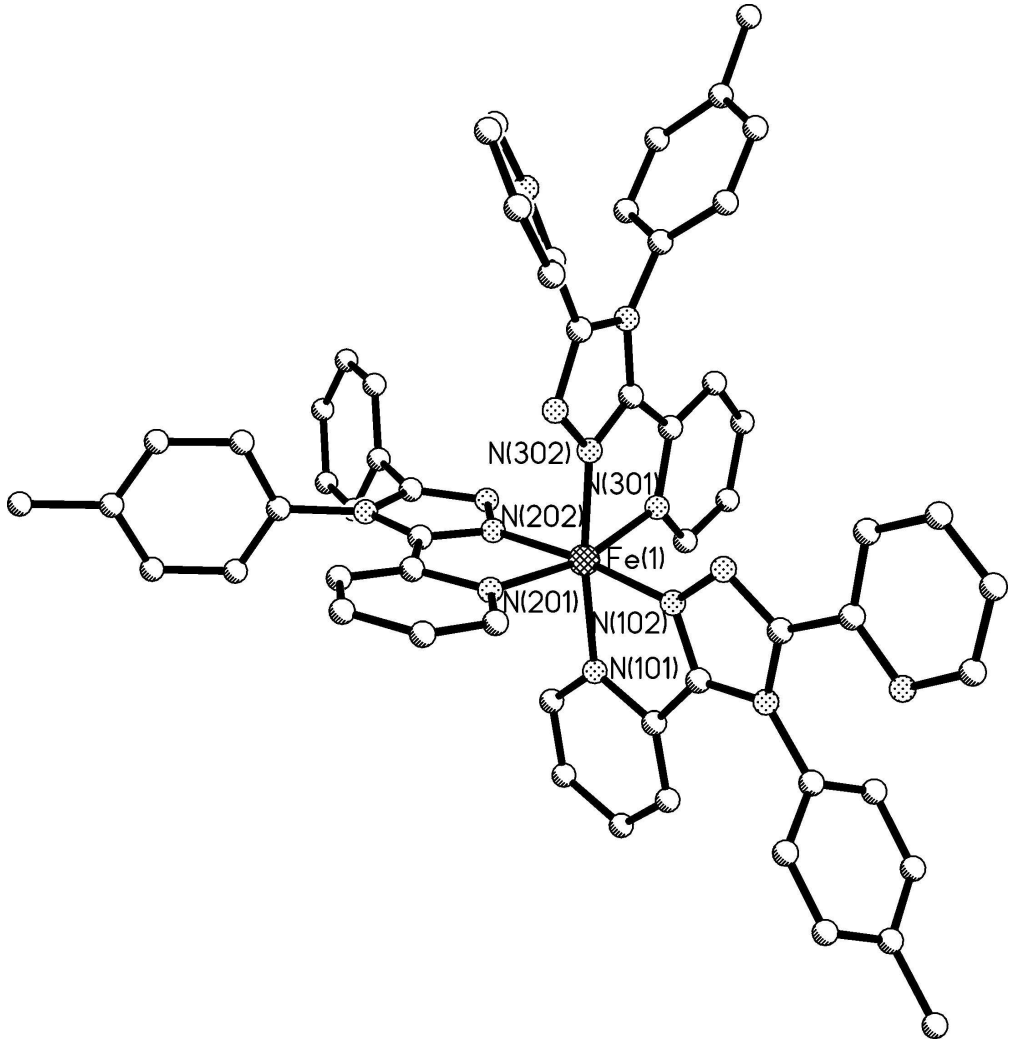
N(302)
N(301)
N(202)
Fe(1)
N(201)
N(102)
N(101)

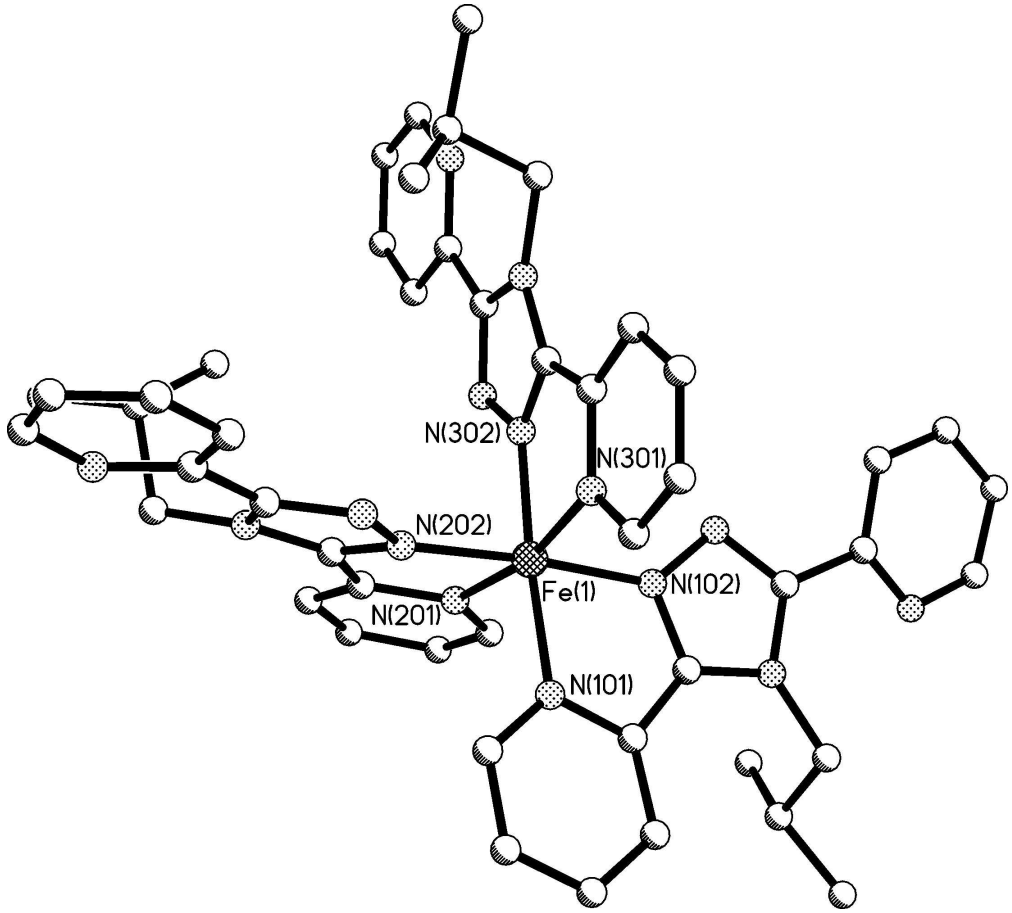
N(302)
N(301)
N(202)
Fe(1)
N(102)
N(201)
N(101)

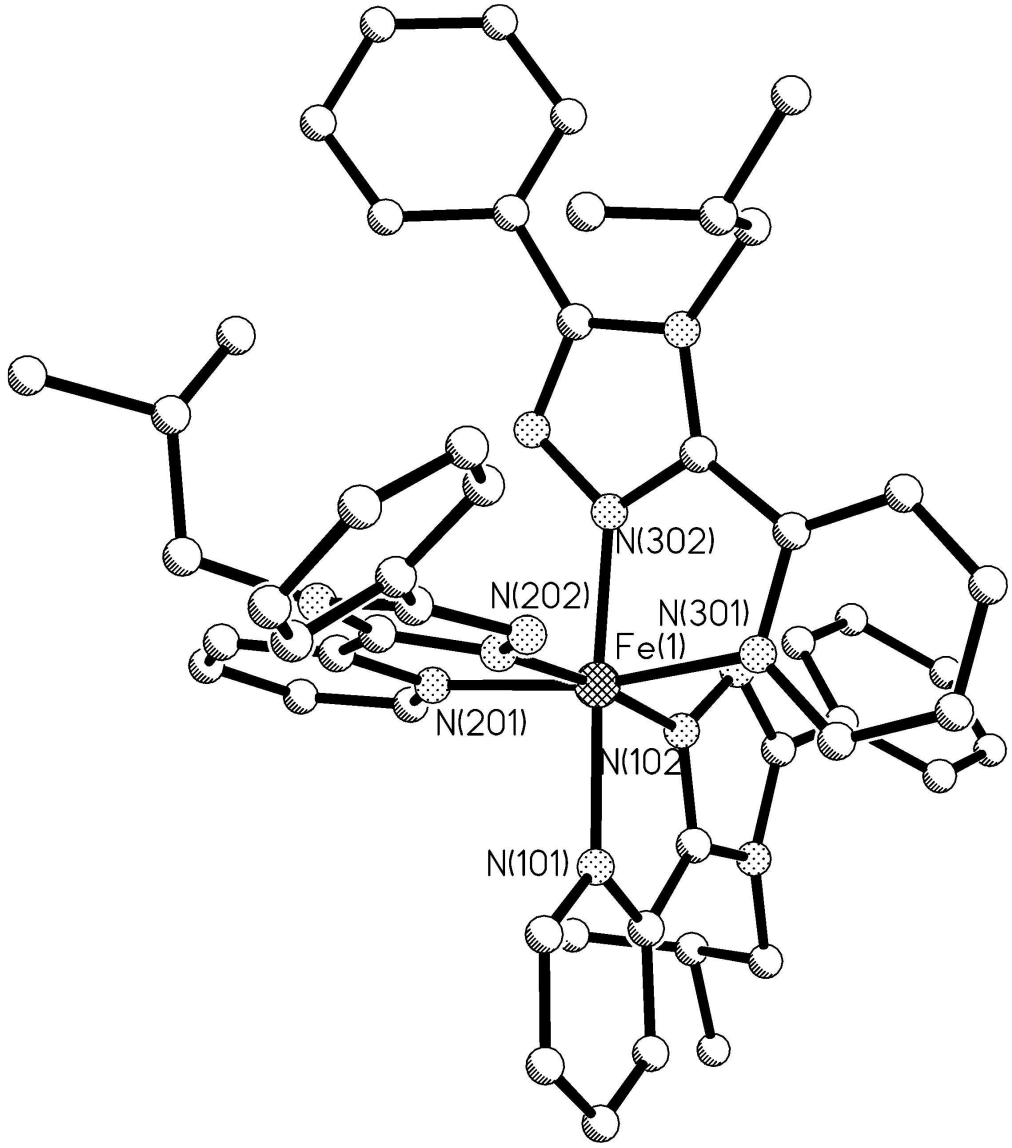
N(302)
N(202)
N(301)
Fe(1)
N(201)
N(102)
N(101)

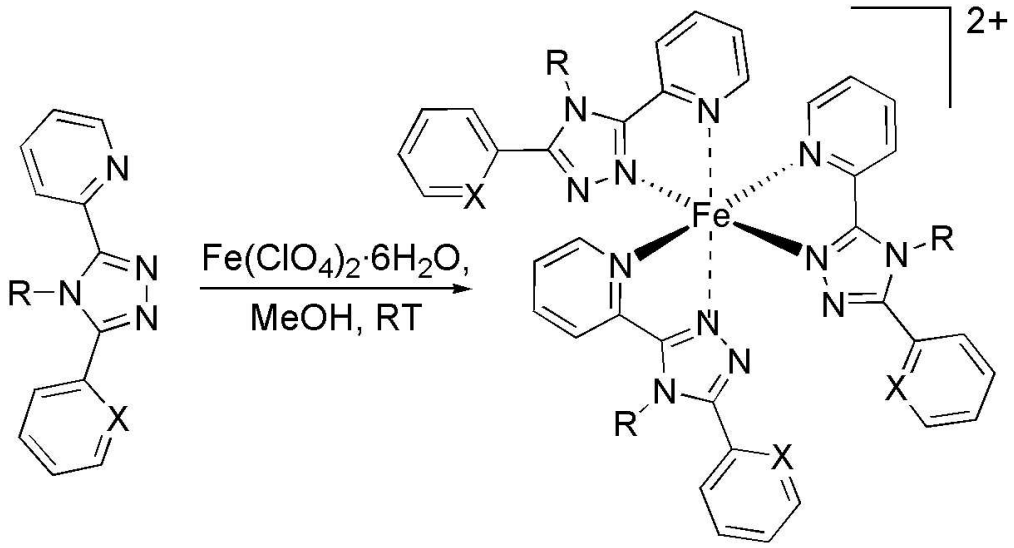

101x55mm (300 x 300 DPI)